Chapter 2

Studies on the monolayer of cholesteric acid

2.1   Introduction

Materials exhibiting thermotropic liquid crystalline phase have been extensively studied as freely suspended films [1] and as Langmuir monolayers at the air-water (A-W) interface [2,3]. Freely suspended thin films of chiral liquid crystals show interesting patterns like stripes and spirals [4, 5]. The modulation of the tilt direction of the molecules leads to the formation of the stripe patterns in the free standing films. The spiral pattern arises due to the spontaneous chiral symmetry breaking [6,7]. Understanding the assembly of such molecules in two-dimensional phase is of fundamental interest and has drawn lot of attention.

In this chapter, we describe our studies on the monolayer properties of a liquid crystalline molecule (cholesteric acid) at the A-W interface. The monolayer was studied using surface manometry, Brewster angle microscope (BAM) and epifluorescence microscope. The effect of the presence of divalent and trivalent ions in the subphase on the monolayer properties have also been studied.

2.2   Experimental

The molecule, 6-(cholest-5-ene-3-lyoxy)-6-oxohexanoic acid (cholesteric acid) was synthesized in the chemistry laboratory of our Institute [8]. The structure of the molecule is shown in Figure. 2.1. The molecule has a sterol moiety as a non-polar hydrophobic group and
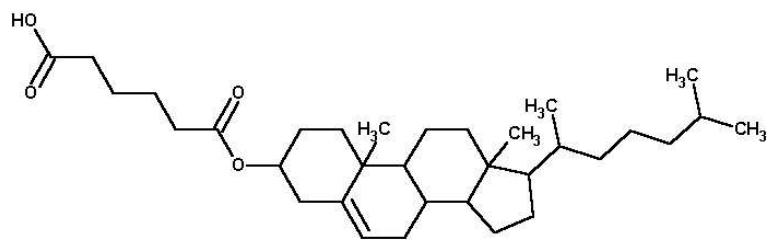
Figure 2.1: Chemical structure of the cholesteric acid (ChA) molecule.

a terminal corboxylic acid polar hydrophilic group. The polar and non-polar groups are separated by an alkyl chain spacer. The surface manometry, epifluorescence and Brewster angle microscopy experiments were carried out under conditions discussed in chapter 1. The divalent or trivalent metal ions containing aqueous subphases were prepared by dissolving $CdCl_2$ or $AlCl_3$ in the ultrapure ion-free water. The salts, $CdCl_2$ and $AlCl_3$ were obtained from Merck. A solution of 1.94 mM concentration of cholesteric acid (ChA) in HPLC grade chloroform was used to spread on the A-W interface. The compression speed of the barriers was maintained at 5.14 ($\mathring{A}^2$/molecule)/minute. The Brewster angle microscope (BAM) images were captured with time using a program written in LabView. The experiments were carried out at room temperature ($\approx$24 °C) and the relative humidity was around 80%.

2.3   Results

Cholesteric acid (ChA) molecule is mesogenic and shows cholesteric phase in the temperature range of 146.7 to 148.5°C on heating. The compound shows the signature of cholesteric phase in the form of an oily streak texture under a polarizing microscope, as shown in Figure 2.2. ChA molecule has many chiral centers and it shows a right-handed specific optical rotation of +231.88°.

2.3.1   Langmuir monolayer of cholesteric acid on ion-free water

The surface pressure (π) - area per molecule (A_m) isotherm of the ChA monolayer on the ultrapure ion-free water is shown in Figure 2.3. The isotherm shows a lift-off area per molecule (A_i) at around 58 $\mathring{A}^2$. There are slope changes in the isotherm at around 57, 52 and
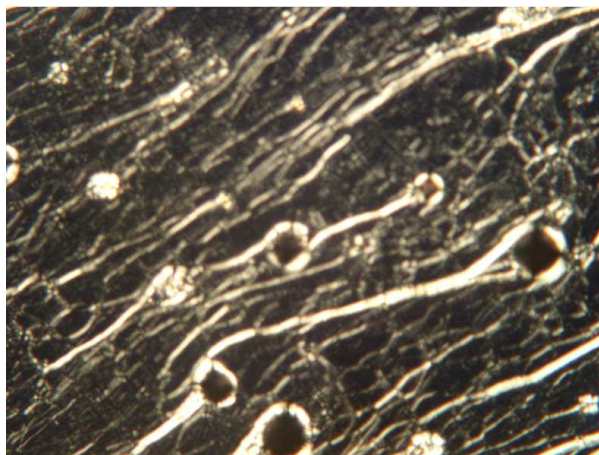
Figure 2.2: Polarizing microscope image showing an oily streak texture of cholesteric acid (ChA) at 147°C.
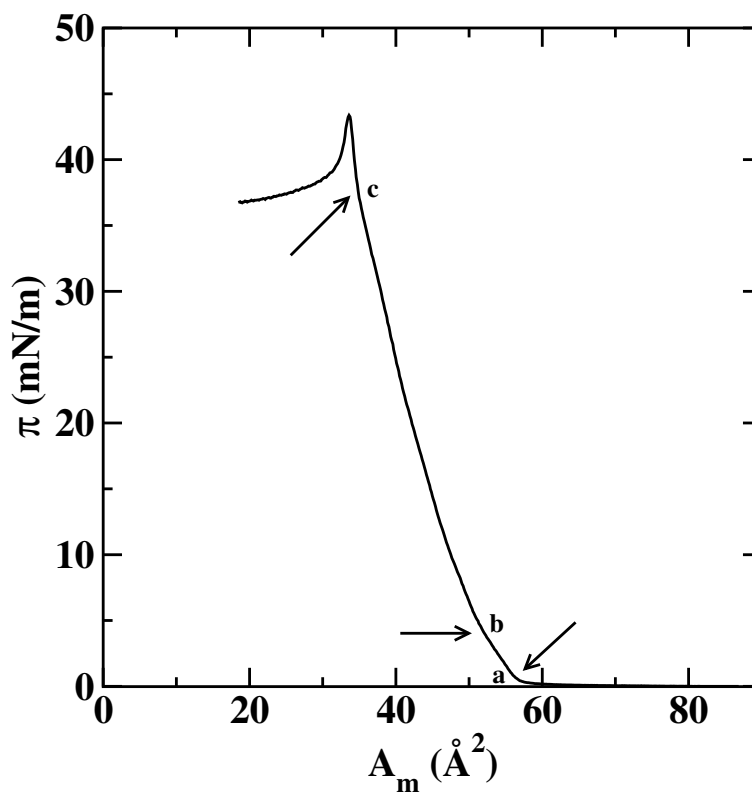
Figure 2.3: Surface pressure (π) - area per molecule (A_m) isotherm of cholesteric acid (ChA) monolayer on the ultrapure ion-free water. The kinks in the isotherm are denoted by the arrows. Their positions in the isotherm are shown by **a, b** and **c**.

35 Å^2. These are indicated by the arrows at the points **a, b** and **c** in the isotherm, respectively. The monolayer collapses at around 33.8 Å^2 with a collapse pressure (π_c) of 43.5 mN/m. In the isotherm, extrapolating the regions **a−b**, **b−c** and **c**−collapse to the zero surface pressure yield the values 56.5, 51.0 and 40.0 Å^2, respectively. The monolayer regions **a−b**, **b−c** and **c**−collapse can be designated as the L$_1'$, L$_2'$ and L$_2$ phases. The trend in the isotherms remains nearly the same with the change in temperature. However, the isotherms shift to the lower area per molecule with the increase in temperature.

The Brewster angle microscope (BAM) images of the ChA monolayer at the A-W interface are shown in Figure 2.4. At a large A$_m$ (Figure 2.4(a)), the ChA monolayer shows a coexistence of gas (dark region) and the L$_1'$ phase (gray background with stripe-like patterns). On compression, the L$_1'$ phase grows at the expense of the gas phase. The L$_1'$ phase shows a pattern consisting of linear stripes, concentric circular stripes and spirals (Figure 2.4(b)). The patterns vanish on compression, leading to a very uniform gray texture of the L$_2'$ phase (Figure 2.4(c)). Further compression does not show any textural change in the BAM images which can distinguish L$_2$ phase from L$_2'$ phase. The monolayer collapses (Figure 2.4(d)) with the formation of three-dimensional (3D) domains (bright domains) which were seen to coexist with L$_2$ phase (uniform gray background).

In the BAM images of L$_1'$ phase, we find the formation of stripes, concentric circular stripes (c) and spirals (s), as depicted in Figure 2.5. Immediately after compressing the monolayer to the L$_1'$ phase, we find a few stripes and small spirals. The number of stripes and the size of the spirals grow with time. Also the spirals rotate with time. We have studied the time evolution of such patterns using BAM. Figure 2.6 shows such BAM images for the ChA in the L$_1'$ phase with time. Here the two images depict the rotation of the spirals. We find the spirals to rotate in the right-handed direction, as indicated by the arrows in the images. The pattern relaxes eventually to an equilibrium state (Figure 2.7). The pattern shows larger spirals and stripes. The stripe width varies in the range of 20 to 100 μm.

We have carried out epifluorescence microscope study on the monolayer of ChA at the A-W interface. The images are shown in Figure 2.8. The epifluorescence image at a large

A$_m$ (Figure 2.8(a)) shows the coexistence of gas (dark domains) and the L$_1^{'}$ phase (gray domains). On compression, the image reveals an uniform gray background indicating an uniform L$_1^{'}$ phase (Figure 2.8(b)). Further compression did not show any change in the texture. Though the BAM imaging reveals a stripe-like pattern and an uniform texture for the L$_1^{'}$ and L$_2^{'}$ phases, respectively, the epifluorescence microscopy did not reveal any difference in the images in the two phases. The image in the collapsed state reveals domains with different gray levels (Figure 2.8(c)) representing thick 3D domains. A lower magnification

(a) A$_m$ = 87.0 Å^2 (b) A$_m$ = 54.7 Å^2
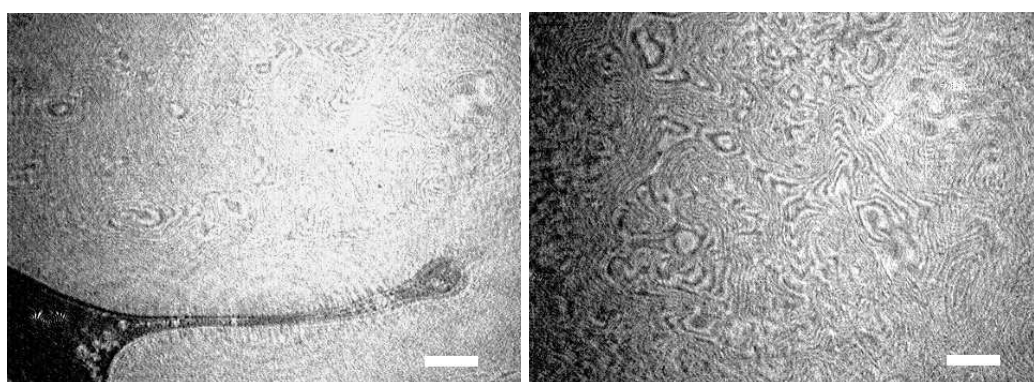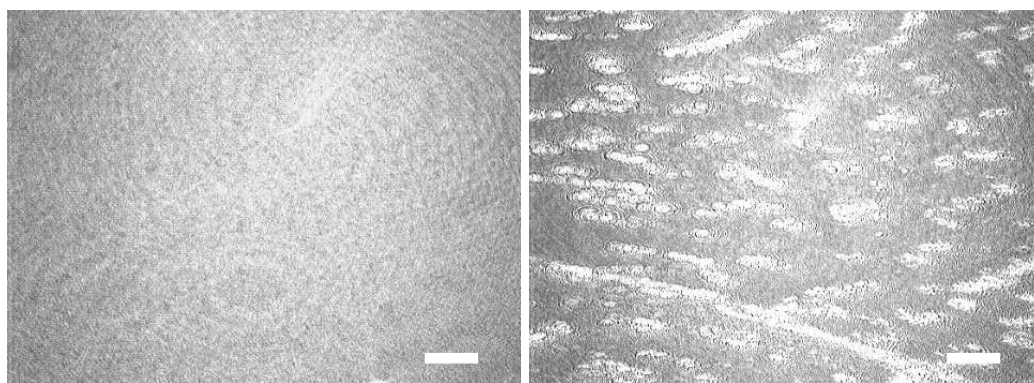
(c) A$_m$ = 47.8 Å^2 (d) A$_m$ = 26.0 Å^2

Figure 2.4: BAM images of the ChA monolayer on the ion-free water captured at different A$_m$. (a) shows a coexistence of gas (dark region) and L$_1^{'}$ phase (gray background with a stripe texture). (b) shows the L$_1^{'}$ phase (stripe texture). (c) shows the L$_2^{'}$ phase (uniform gray background). The image shows concentric ellipses in the background which are artifacts arising due to scattering of laser light from very fine dust particles on the lens and polarizer of the microscope. Such features appear prominently in the images with uniform background. (d) shows a collapsed state. Here 3D domains (bright domains) coexist with the L$_2$ phase (gray background). The scale bar represents 500 μm.
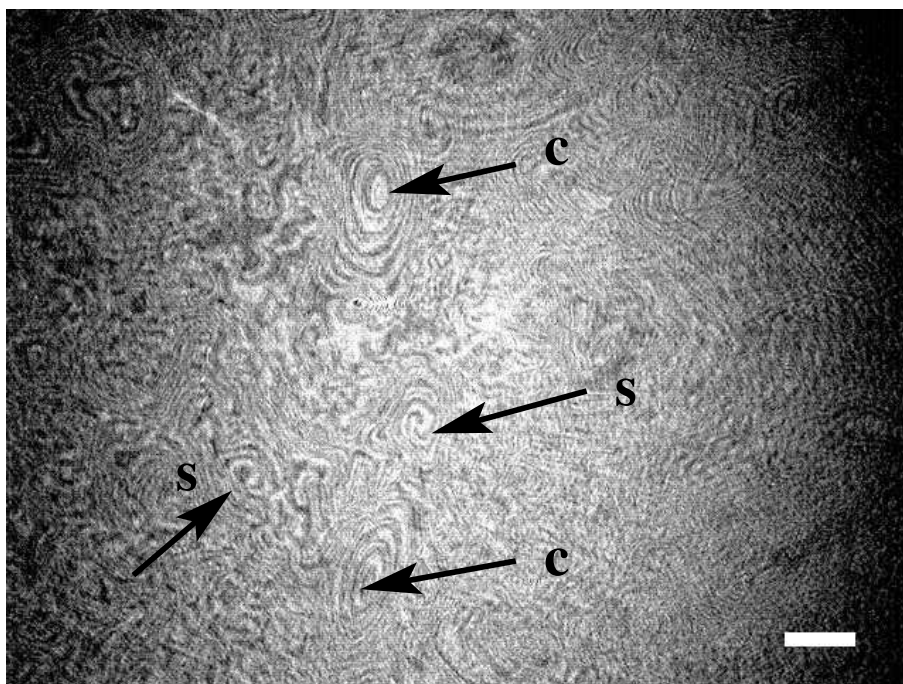
Figure 2.5: BAM image of the ChA monolayer on the ion-free water captured immediately after holding the barriers at an A_m of 54 Å^2. The arrows in the image are drawn to show the spirals (s) and concentric circular stripes (c). The scale bar represents 500 μm.
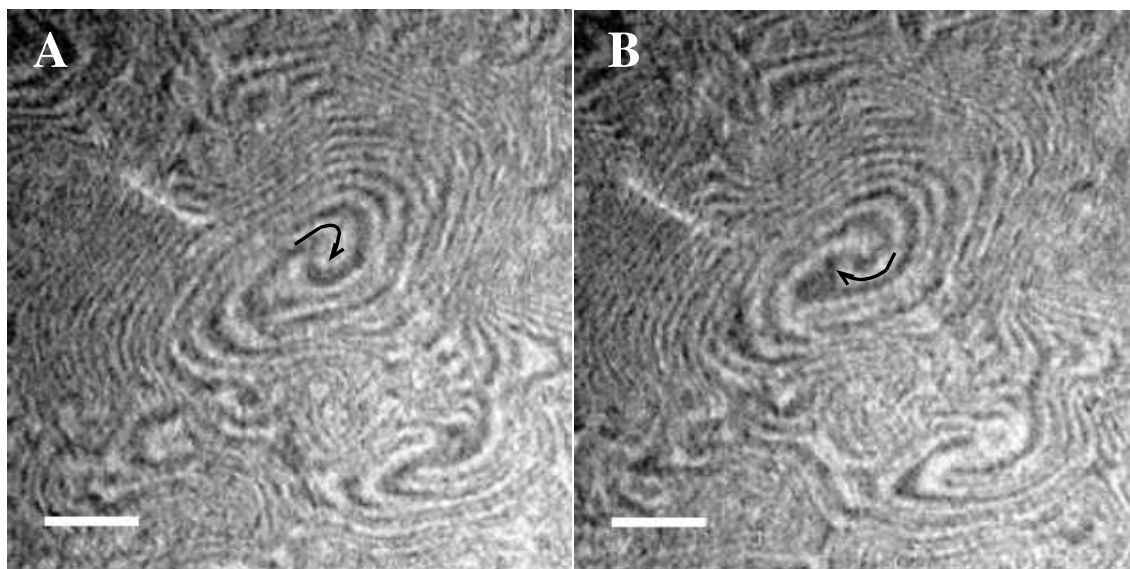
Figure 2.6: BAM images of the ChA monolayer on the ion-free water captured at an A_m of 54 Å^2 after four minutes of holding the barriers. The time interval between images A and B is two seconds. The arrow on one arm of the spiral is drawn to show its sense of rotation. The scale bar represents 335 μm.

Figure 2.7: BAM image of the ChA monolayer on the ion-free water captured at an A_m of 54 $\mathring{A}^2$ after 24 hours of holding the barriers. The scale bar represents 500 μm.

(a) $A_m = 60.0$ Å^2

(b) $A_m = 54.7$ Å^2

(c) $A_m = 29.0$ Å^2
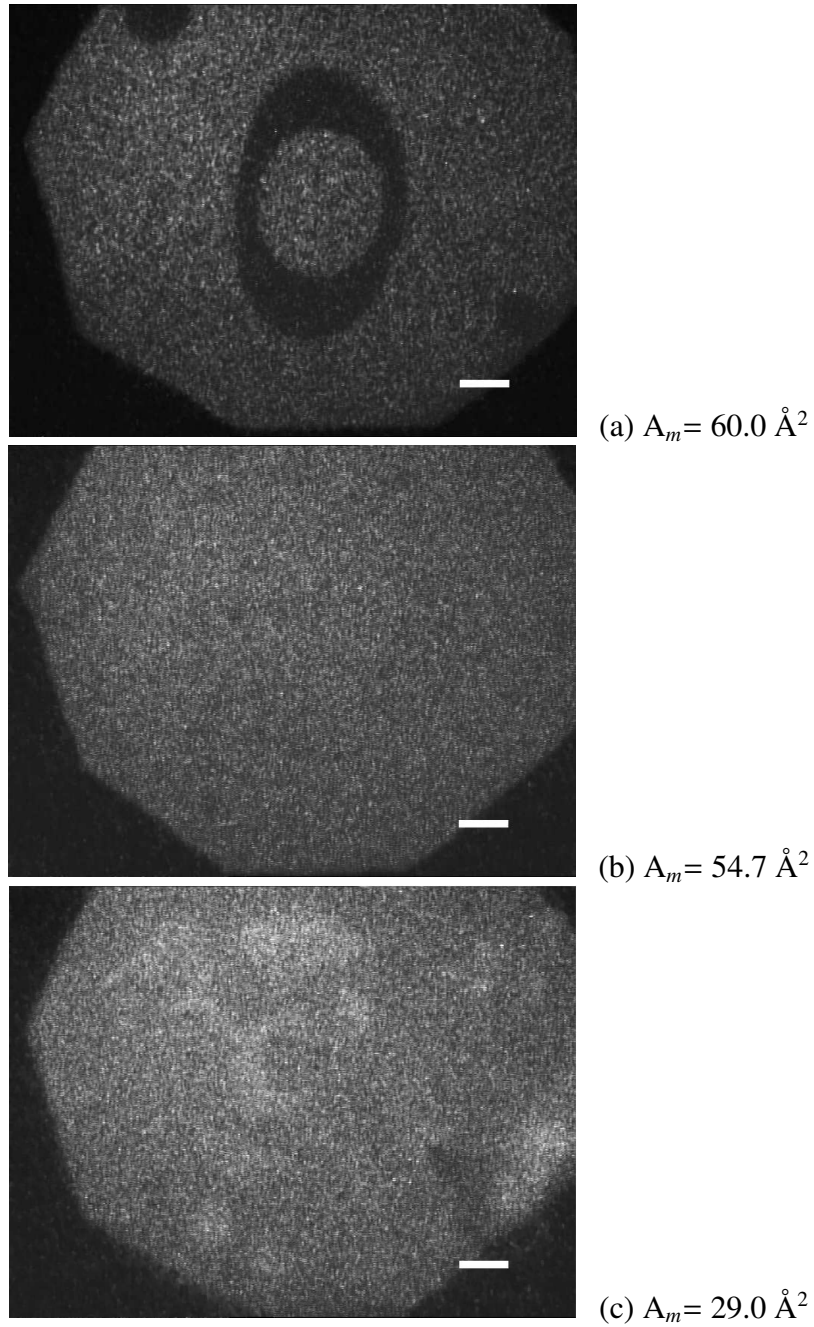
Figure 2.8: Epifluorescence images of the ChA monolayer on the ion-free water captured at different A_m. (a) shows a coexistence of the gas (dark region) and the $L_1^{'}$ phase (gray domains). (b) shows an uniform $L_1^{'}$ phase (uniform gray texture). (c) shows the collapsed state. In the collapsed state, the image reveals the regions with different gray levels representing the 3D domains of various thickness. The scale bar represents 25 μm.
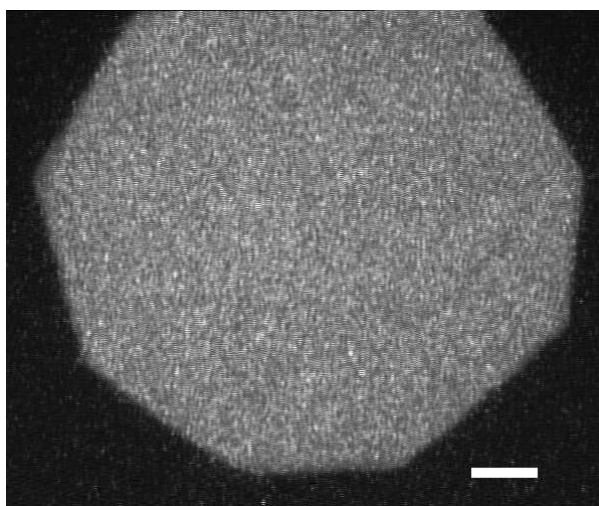
Figure 2.9: Epifluorescence image of the ChA monolayer on the ion-free water captured in the L_1' phase (A_m = 54 Å^2) with a lower magnification. The gray uniform texture represents the uniform L_1' phase. The scale bar represents 312 μm.

epifluorescence microscope image of the ChA monolayer in the L_1' phase is shown in Figure 2.9. The image shows an uniform texture for the L_1' phase.

2.3.2 Metal complexes of cholesteric acid monolayer

We have studied the effects of divalent (Cd^{2+}) and trivalent (Al^{3+}) metal ions in the subphase on the monolayer properties of ChA. The isotherms of the monolayers on the aqueous subphases containing different molar concentrations of $CdCl_2$ are shown in Figure 2.10. The isotherm for the very low concentration (1.76×10^{-6} M) of $CdCl_2$ in the aqueous subphase shows a trend similar to that of ChA monolayer on the ion-free water. However, the isotherm shows a small shift in the A_i to the lower value. The isotherms at the higher concentration show almost a constant value of A_i (~49 Å^2). Unlike the case of ChA on ion-free water which shows three slope changes corresponding to three different phases, here the isotherms reveal two slope changes (shown by the arrows in the isotherm of 1.76×10^{-4} M of $CdCl_2$ in the subphase) indicating two phases. The collapse pressure increases by about 3 to 4 mN/m due to the $CdCl_2$ in the subphase. The nature of the collapse is also different, and it showed a plateau rather than a sharp drop in surface pressure. The value of the limiting area per molecule (A_o) for the higher concentrations lies in the range of 36 to 38 Å^2. This

31
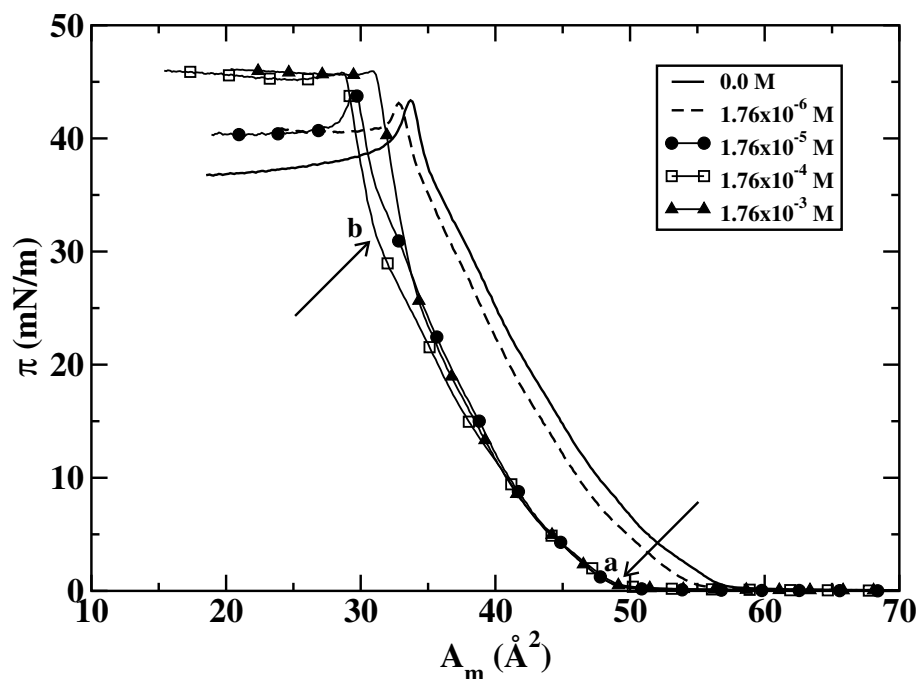
Figure 2.10: Surface pressure (π) - area per molecule (A_m) isotherms of ChA monolayer on the aqueous subphase containing different molar concentrations of $CdCl_2$. Arrows are drawn in one of the isotherms to indicate the kinks.

value approximately corresponds to the cross-sectional area of the molecule for its normal orientation at the interface. The extent of the steep region of the isotherms increases with increasing concentration of $CdCl_2$ in the subphase.

The BAM images of the monolayer of ChA with 1.76×10^{-4} M of $CdCl_2$ in the subphase are shown in Figure 2.11. The image shows the coexistence of the dark region (gas phase) and a gray texture at a large A_m (Figure 2.11(a)). On compression, the dark region disappears and the monolayer shows a homogeneous gray texture (Figure 2.11(b)). On further compression, the images do not show any change in the texture. The monolayer collapses (Figure 2.11(c)) with the formation of 3D structures (bright domains) coexisting with a gray background. The features (stripe-like patterns) corresponding to the $L_1^{'}$ phase of the ChA monolayer on the ion-free water was not observed. The epifluorescence images of ChA monolayer on $CdCl_2$ containing subphase show a coexistence of the gas (dark region) and a condensed phase (gray region) at a large A_m (Figure 2.12(a)). Compression of the monolayer leads to an uniform texture (Figure 2.12(b)). On further compression,
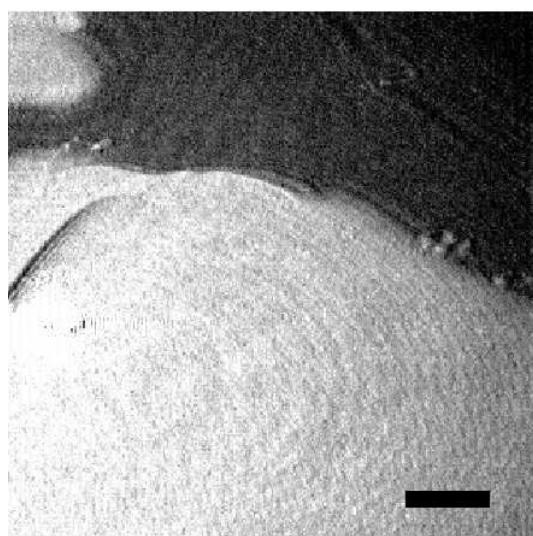
(a) $A_m = 51.0$ Å^2
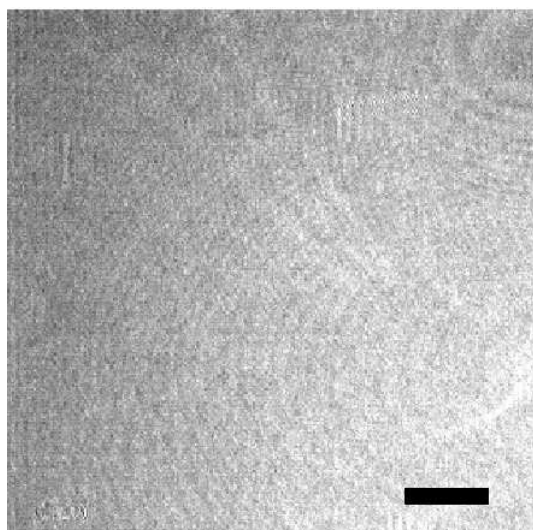
(b) $A_m = 33.6$ Å^2
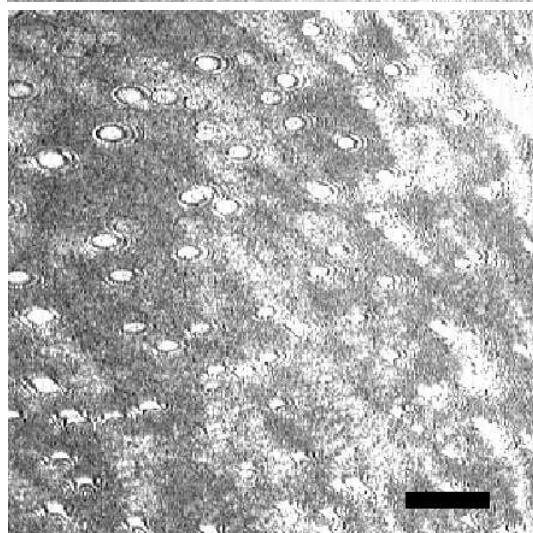
(c) $A_m = 25.0$ Å^2

Figure 2.11: BAM images of the ChA monolayer on an aqueous subphase containing 1.76×10^{-4} M of CdCl$_2$ captured at different A_m. (a) shows a coexistence of gas (dark region) and a condensed phase (gray domains). (b) shows an uniform condensed phase (gray background). (c) shows a collapsed state where 3D structures (bright domains) are seen to coexist with a gray background. The scale bar represents 500 μm.

(a) $A_m = 62.7$ Å^2

(b) $A_m = 34.3$ Å^2

(c) $A_m = 25.0$ Å^2
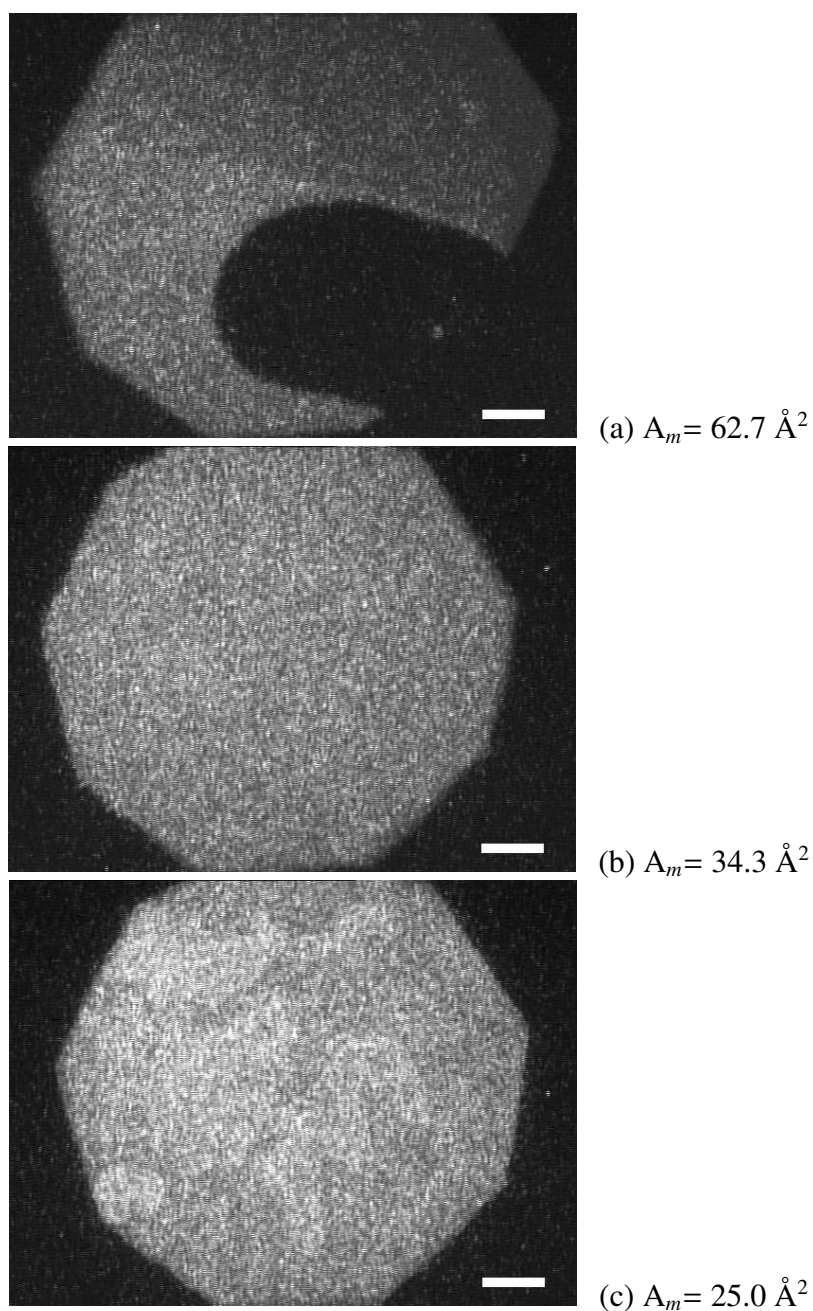
Figure 2.12: Epifluorescence images of the ChA monolayer on an aqueous subphase containing 1.76×10^{-4} M of CdCl$_2$ captured at different A_m. (a) shows a coexistence of gas (dark region) and a condensed phase (gray domains) and (b) shows an uniform condensed phase (gray background). (c) shows the collapsed state. In the collapsed state, the domains with different intensity levels represent thick domains. The scale bar represents 50 μm.

the monolayer collapses. The collapsed state shows the 3D domains of different intensity levels (Figure 2.12(c)). The different intensity levels indicate the domains of different thicknesses.

The effects of the trivalent metal ion (Al^{3+}) in the subphase on the surface pressure - area per molecule isotherms of ChA monolayer are shown in Figure 2.13. The isotherms of
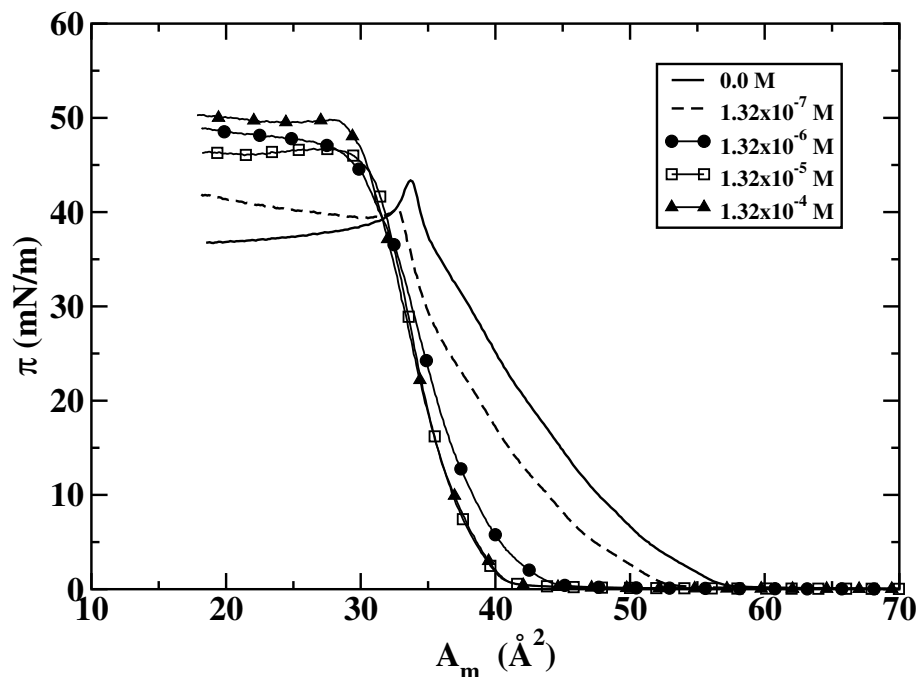
Figure 2.13: Surface pressure (π) - area per molecule (A_m) isotherms of the ChA monolayer for different molar concentrations of $AlCl_3$ in the aqueous subphase.

ChA on the $AlCl_3$ containing subphase show a comparatively large shift in the A_i to the lower values. The isotherms show a steep rise in surface pressure corresponding to a transition from the coexistence of gas and a condensed phase to the condensed phase. The isotherms indicate only one condensed phase. The A_o value lies in the range of 38 to 39 $\AA^2$ indicating a normal orientation of the molecules. The collapse pressure increases with increasing concentration of $AlCl_3$. The nature of collapse shows a plateau rather than a sharp drop in surface pressure in the isotherms.

The BAM images of ChA monolayer on $AlCl_3$ containing aqueous subphase are shown in Figure 2.14. The image (Figure 2.14(a)) shows a coexistence of the gas (dark region) and a condensed phase (gray background). On compression, an uniform gray texture
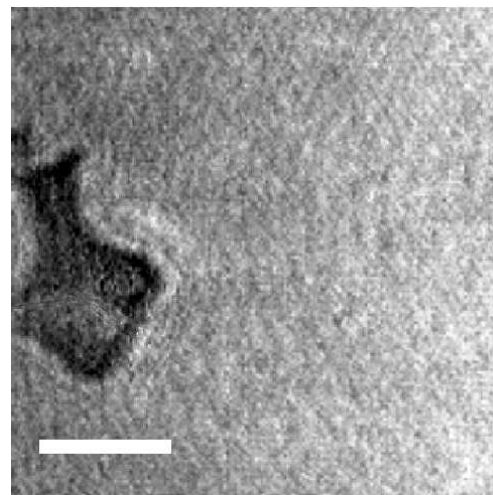
(a) $A_m = 44.0$ Å^2
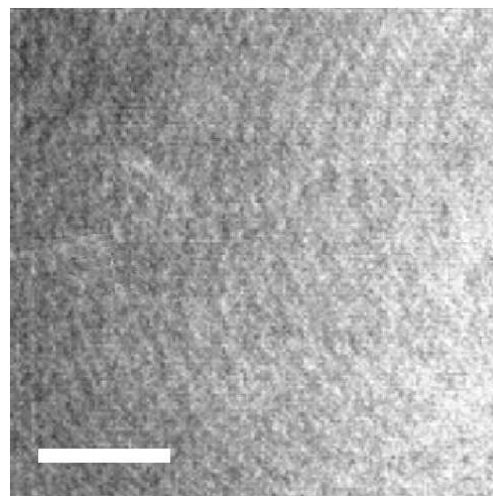
(b) $A_m = 31.0$ Å^2
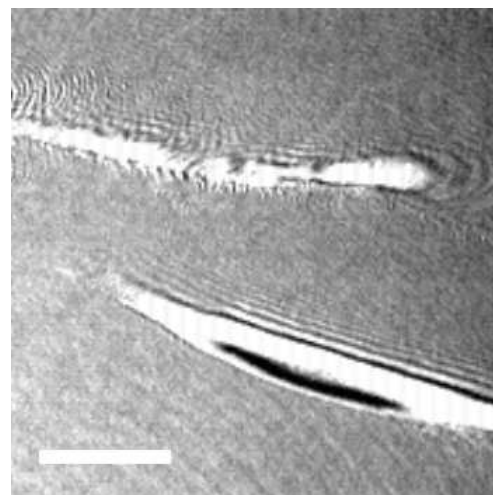
(c) $A_m = 22.0$ Å^2

Figure 2.14: BAM images of the ChA monolayer on an aqueous subphase containing 1.32×10^{-5} M of AlCl$_3$ captured at different A_m. (a) shows a coexistence of gas (dark region on the left side of the image) and the condensed phase (gray regions). (b) shows an uniform condensed phase (gray background) and (c) shows a coexistence of condensed phase (gray background) and 3D bright streaks representing 3D crystals in the collapsed state. The images show part of concentric ellipses in the background which are artifacts arising due to scattering of laser light from very fine dust particles on the lens and polarizer of the microscope. Such features appear prominently in the images with uniform background. The scale bar represents 500 μm.

36

(Figure 2.14(b)) of the condensed phase was observed. The collapsed state shows bright streak-like 3D crystalline structures (Figure 2.14(c)) coexisting with the condensed phase (gray background). The characteristic stripe-like pattern of the L_1' phase was not observed during BAM imaging of ChA monolayer on $AlCl_3$ containing aqueous subphase. Figure 2.15 shows the epifluorescence images of the ChA monolayer on $AlCl_3$ containing aqueous subphase. The phases indicated by the epifluorescence images are consistent with those indicated by the BAM images. At large A_m, the image (Figure 2.15(a)) reveals a coexistence of the gas (dark domains) and a condensed phase (gray regions). Compression of the monolayer leads to an uniform texture of the condensed phase (Figure 2.15(b)). The collapsed state shows a very bright streak-like crystalline domain (Figure 2.15(c)) coexisting with the condensed phase (gray background). The 3D crystalline streaks were immobile. However, in the case of ChA on $CdCl_2$ containing aqueous subphase, the collapsed state shows 3D structures of small droplets which were mobile and fluidic.

2.4   Discussion

The ChA molecule (Figure 2.1) is structurally similar to the cholesterol molecule. In the case of ChA, the size of the carboxylic polar group is around 2 Å, whereas the sterol non-polar group is around 5 Å. Such mismatch in the sizes of the polar and non-polar groups is known to induce a tilt of the molecules in the monolayer at the A-W interface [9–11].

The isotherm of ChA on ion-free water reveals three kinks, indicating three phases. The large extrapolated A_m (56.5 Å^2) of the region of the isotherm **a−b** (Figure 2.3) can be accounted for by the tilt of the molecules in the monolayer. It is known from literature that the different intensity levels seen in the BAM images are due to a variation in tilt-azimuth of the molecules in the monolayer, whereas an uniform pattern is attributed to an uniform orientational state of the molecules [12, 13]. The intensity modulation in the observed BAM images (Figure 2.4(b)), giving rise to stripe patterns, can be attributed to the tilt-azimuthal variation of the molecule in the monolayer. The stripe patterns of the ChA monolayer observed under BAM appear liquid-like. Hence, this phase can be considered as a liquid-like

(a) $A_m = 87.0$ Å^2

(b) $A_m = 34.3$ Å^2

(c) $A_m = 19.0$ Å^2
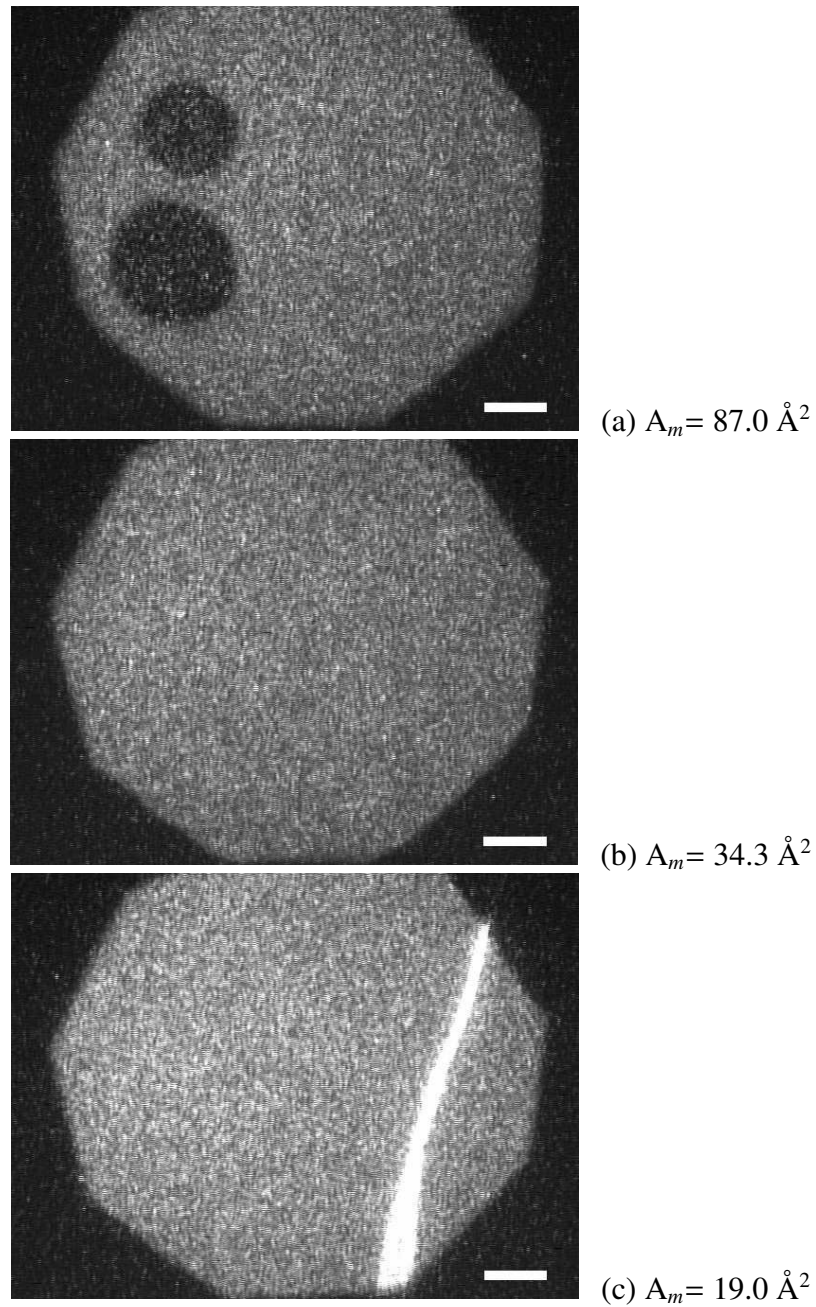
Figure 2.15: Epifluorescence images of the ChA monolayer on an aqueous subphase containing $1.32{\times}10^{-5}$ M of AlCl$_3$ captured at different A_m. (a) shows a coexistence of gas (dark domains) and a condensed phase (gray background). (b) shows an uniform condensed phase (uniform gray background). (c) shows a coexistence of condensed phase (gray background) and a bright streak-like domain in the collapsed state. The scale bar represents 50 μm.

phase with varying tilt-azimuth of the molecules. We have assigned this phase as $L_1^{'}$ phase.

The phase corresponding to the region **b**−**c** of the isotherm (Figure 2.3) also shows large value of extrapolated A_m(51.0 Å^2). This suggests a tilt of the molecules in the monolayer in this phase. A very uniform texture, as observed in the BAM image (Figure 2.4(c)), suggests an uniform orientation of the molecules in this phase. Also the BAM image indicates a liquid-like phase. Hence, this phase may be considered as a liquid phase with uniformly tilted molecules. We have assigned this phase as $L_2^{'}$ phase. The phase corresponding to the region **c**−collapse in the isotherm (Figure 2.3) yields the extrapolated $A_m$value to be 40 Å^2. This value approximately corresponds to the cross-sectional area of the molecule for its normal orientation. Therefore, this phase can be considered as a condensed phase with untilted molecules (L_2 phase). BAM images in this phase show an uniform texture indicating an uniform orientation of the molecules.

Tabe *et al.* have shown that a simultaneous imaging of a monolayer using a linear- and circular-depolarized reflected light microscope (DRLM) yields information of the tilt and azimuthal variation of the molecules in the monolayer [14]. They considered a geometry (Figure 2.16) where the molecule tilts at an angle θ with respect to the surface normal ($\hat{Z}$). The tilt direction on the layer plane (XY) is represented by a vector $\vec{c}$. The vector
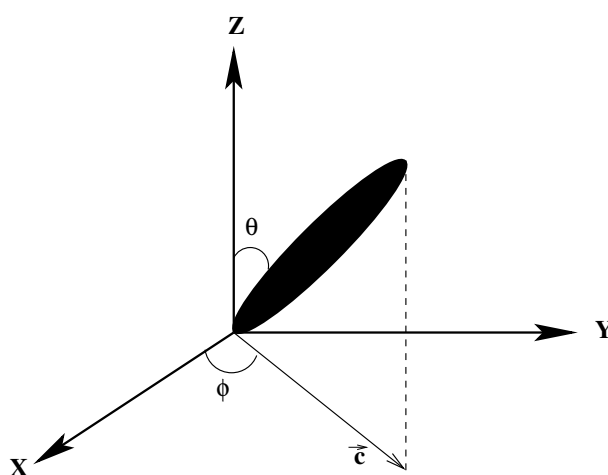
Figure 2.16: The geometry of a tilted molecule in the monolayer at the A-W interface. The projection of the tilted molecule on the layer plane (XY) is denoted by a vector, $\vec{c}$. The angles θ and ϕ represent the tilt of the molecule with respect to the surface normal and the azimuthal angle with respect to the X axis.

$\vec{c}$ makes an angle ϕ with X-axis. The tilt and the azimuthal variation were extracted from the intensity data of circular- and linear-DRLM, respectively [15]. They showed that the reflected intensity (I_L) from linear-DRLM is proportional to $\sin^2(\phi)\cos^2(\phi\text{-}F)$, where the parameter F depends on the dielectric constant of the sample and the tilt angle of the molecule. F can be considered as a constant for an uniformly tilted molecule. Hence, the reflected intensity depends on the orientational angle ϕ [15]. The geometry of our BAM imaging is similar to the one reported for the linear-depolarized reflected light microscopy except that the angle of incidence in their case is almost normal to the interface [14], whereas in BAM, it is at Brewster angle for A-W interface. Hence, the intensity variation in our BAM imaging can correspond to a variation of the azimuthal angle of the tilted molecules. The intensity, I_L is minimum if the vector $\vec{c}$ is along the plane of incidence (XZ) or perpendicular (YZ) to it. These conformations of the molecules contribute to the dark regions in the stripe and spiral patterns as discussed above. However, the maximum intensity region of the stripes and the spiral corresponds to a value of ϕ to be $n\pi/4$, where n is an integer. According to the theory proposed by Tabe and Yokoyama, two bright stripes separated by the dark region occur for a complete period of rotation of ϕ [15].

The origin of stripes and the spirals observed from the BAM imaging of the monolayer of ChA in $L_1^{'}$ phase due to a variation in surface density can be ruled out from the epifluorescence microscope (with low magnification) images showing a larger monolayer area (Figure 2.9). Here the scale of the image is comparable to that of the BAM images. The miscibility of a dye molecule in a Langmuir monolayer phase is dependent on the surface density of the phase. Therefore, any density variation would have led the variation in the fluorescence intensity. The absence of any such variation in the fluorescence intensity (Figure 2.9) suggests that the formation of stripes and the spiral in the BAM images are due to the tilt-azimuthal variation rather than the density variation.

Using polarized fluorescence [10], Brewster angle [9] and depolarized reflected light microscopy [16], stripes and spirals have been observed in the Langmuir monolayer of non-chiral and chiral molecules. Recent report on the Langmuir monolayer of a ferroeletric

chiral liquid crystal shows the stripes and the spirals in the multilayer regime of the isotherm. However, the monolayer region reveals uniform tilted phase without any bireferengence [17].

In a theoretical description given by Selinger and Selinger [18], the asymmetry in sizes of polar (head) and non-polar (tail) groups leads the molecules to tilt at the interface. For a constant tilt, a modulation in $\vec{c}$ gives rise to a stripe pattern in the BAM or polarized fluorescence microscope (PFM) images of a monolayer at the interface. The presence of a point defect in $\vec{c}$ of the molecules in the monolayer leads to the appearance of spirals in the BAM or PFM images. They find that the circular concentric stripes are the degenerate state of the spirals, and hence both can coexist. They have suggested that the sense of rotation of the spirals to be random. Using epifluorescence microscopy, Krüer and Lösche have demonstrated that the macroscopic curvature of lobes (hands) of the spiral domains formed by the chiral molecules at the A-W interface is strongly dependent on the enantiomeric constitution of the molecule [19]. The curvature reduces gradually with the increase in enantiomers and vanishes for the racemate [20]. In the BAM imaging of the ChA monolayer in the L_1' phase, we observed a coexistence of concentric stripes and spirals. We find the spirals to rotate right-handedly. The ChA is an optically active right-handed molecule. Therefore, the rotation of the spirals may be related to the molecular handedness.

The presence of a metallic ion in the subphase forms a complex with the fatty acid molecules in the monolayer. It is known from the literature that a Cd^{2+} ion forms a complex with two stearic acid molecules in order to achieve electroneutrality. Similar complex formation takes place with a trivalent metal ion [21]. Since the ChA molecule possesses a terminal carboxylic head group, it is more likely to form such complexes with the divalent (Cd^{2+}) and trivalent (Al^{3+}) metal ions at the A-W interface.

The non-appearance of the stripe-like patterns in the BAM imaging of the ChA monolayer on the $CdCl_2$ containing aqueous subphase suggests the suppression of the L_1' phase. The ChA monolayer on the $CdCl_2$ containing subphase shows two kinks in the isotherms (Figure 2.10) representing two phases. The large extrapolated area per molecule ($\sim$45 to 42 Å^2) of the region of the isotherm **a−b** suggests that the molecules are tilted in

41

the monolayer. The BAM and epifluorescence imaging in this region show a very uniform texture. This phase may be considered as an uniformly tilted liquid phase ($L_2^{'}$) of the complex of the ChA and $CdCl_2$. The value of extrapolated A_m (A_o) of the steep region of the isotherm (region **b**−collapse) indicates a normal orientation of the complex molecule of ChA and $CdCl_2$ in this phase. We assigned this phase as L_2 phase. The smaller values of A_o for the complex as compared to that of ChA on the ion-free water indicate a condensation effect of the $CdCl_2$ on the L_2 phase of the monolayer.

The monolayer of ChA on $AlCl_3$ containing aqueous subphase (Figure 2.13) exhibits only one condensed phase in which the complex molecule of ChA and $AlCl_3$ may orient normal to the interface (L_2 phase). The non-appearance of the stripe-like patterns in the BAM imaging indicates the suppression of $L_1^{'}$ phase.

Due to the incorporation of the metal ions in the aqueous subphase, the ChA monolayer shows shifts of the isotherms to the low A_m suggesting a condensation effect. This is due to the complexation of ChA with the ions. The ChA monolayer on $CdCl_2$ containing aqueous subphase shows the $L_2^{'}$ and L_2 phases where the extent of the L_2 phase increases with increasing concentration of the Cd^{2+} ions. The presence of $AlCl_3$ in the aqueous subphase suppresses the tilted $L_2^{'}$ phase and shows only the untilted condensed phase (L_2) of the complex molecule.

2.5   Conclusions

The monolayer studies of ChA reveal many interesting results. The manometry studies indicate the existence of gas, $L_1^{'}$, $L_2^{'}$, L_2 and a collapsed state. The BAM imaging of the monolayer in the $L_1^{'}$ phase reveals the patterns like stripes and spirals. The origin of such texture is attributed to the tilt-azimuthal variation of the molecules in the monolayer. The formation of stripes may arise due to a mismatch in sizes of the polar (head) group and non-polar (tail) group of the molecules. The presence of a point defect in the monolayer leads to the formation of spirals, as seen in the BAM images. The right-handed rotation of the spirals may be due to the molecular chirality. The $L_2^{'}$ phase shows a uniform texture in both

the microscopy techniques. This is due to the uniform tilt of the molecules in this phase. We suggest that the L_2 phase is an untilted condensed phase. We find that the ChA monolayer on $CdCl_2$ containing aqueous subphase suppresses $L_1^{'}$ phase, whereas the monolayer on $AlCl_3$ containing subphase suppresses both $L_1^{'}$ and $L_2^{'}$ phases. On the other hand, the untilted condensed (L_2) phase gets stabilized due to the presence of metal ions.

Bibliography

[1] A. A. Sonin, *Freely Suspended Liquid Crystalline Films* (John Wiley and Sons Ltd, England, 1999).

[2] M. F. Daniel, O. C. Lettington, and S. M Small, Thin Solid Films **99**, 61 (1983).

[3] F. Rondelez, D. Koppel, and B. K. Sadashiva, J. Phys. (Paris) **43**, 1361 (1982).

[4] S. A. Langer and J. P. Sethna, Phys. Rev. A **34**, 5035 (1986).

[5] S. B. Dierker, R. Pindak, and R. B. Meyer, Phys. Rev. Lett. **56**, 1819 (1986).

[6] J. V. Selinger, Z. G. Wang, R. F. Bruinsma, and C. M. Knobbler, Phys. Rev. Lett. **70**, 1139 (1993).

[7] K. Pang and N. A. Clark, Phys. Rev. Lett. **73**, 2332 (1994).

[8] Sandeep Kumar (To be published).

[9] S. Rivière, S. Hénon, and J. Meunier, Phys. Rev. E **49**, 1375 (1994).

[10] X. Qiu, J. Ruiz-Garcia, K. J. Stine, C. M. Knobbler, and J. V. Selinger, Phys. Rev. Lett. **67**, 703 (1991).

[11] S. A. Safran, M. O. Robbins, and S. Garoff, Phys. Rev. A **33**, 2186 (1986).

[12] J. Meunier, Colloids and Surf. A **171**, 33 (2000).

[13] J. Ignes-Mullol and D.K. Schwartz, Nature (London) **410**, 348 (2001).

[14] Y. Tabe, N. Shen, E. Mazur, and H. Yokoyama, Phys. Rev. Lett. **82**, 759 (1999).

[15] Y. Tabe and H. Yokoyama, Langmuir **11**, 699 (1995).

[16] Y. Tabe and H. Yokoyama, J. Phys. Soc. Jpn. **63**, 2472 (1994).

[17] J. -L. Gallani, S. Mery, Y. Galerne, and D. Guillon, J. Phys. Chem. B **108**, 11627 (2004).

[18] J. V. Selinger and R. L. B. Selinger, Phys. Rev. E **51**, R860 (1995).

[19] P. Krüger and M. Lösche, Phys. Rev. E **62**, 7031 (2000).

[20] In chemistry, a racemate is a mixture of equal amounts of left- and right-handed stereoisomers of a chiral molecule.

[21] G. L. Gaines, Jr., *Insoluble Monolayers at Liquid-Gas Interfaces* (Wiley-Interscience, New York, 1966).